nature physics

LETTERS

https://doi.org/10.1038/s41567-018-0328-0

There are amendments to this paper

Design and characterization of electrons in a fractal geometry

S. N. Kempkes[1,3], M. R. Slot[2,3], S. E. Freeney[2], S. J. M. Zevenhuizen[2], D. Vanmaekelbergh[2], I. Swart[2*] and C. Morais Smith[1*]

The dimensionality of an electronic quantum system is decisive for its properties. In one dimension, electrons form a Luttinger liquid, and in two dimensions, they exhibit the quantum Hall effect. However, very little is known about the behaviour of electrons in non-integer, or fractional dimensions[1]. Here, we show how arrays of artificial atoms can be defined by controlled positioning of CO molecules on a Cu (111) surface[2–4], and how these sites couple to form electronic Sierpiński fractals. We characterize the electron wavefunctions at different energies with scanning tunnelling microscopy and spectroscopy, and show that they inherit the fractional dimension. Wavefunctions delocalized over the Sierpiński structure decompose into self-similar parts at higher energy, and this scale invariance can also be retrieved in reciprocal space. Our results show that electronic quantum fractals can be artificially created by atomic manipulation in a scanning tunnelling microscope. The same methodology will allow future studies to address fundamental questions about the effects of spin–orbit interactions and magnetic fields on electrons in non-integer dimensions. Moreover, the rational concept of artificial atoms can readily be transferred to planar semiconductor electronics, allowing for the exploration of electrons in a well-defined fractal geometry, including interactions and external fields.

Fractals have been investigated in a wide variety of research areas, ranging from polymers[5], porous systems[6], electrical storage[7] and stretchable electronics[8] down to molecular[5,9–11] and plasmonic[12] fractals. On the quantum level, fractal properties emerge in the behaviour of electrons under perpendicular magnetic fields; for example, in the Hofstadter butterfly[13] and in quantum Hall resistivity[14,15]. In addition, a multi-fractal behaviour has been observed for the wavefunctions at the transition from a localized to delocalized regime in disordered electronic systems[16–18]. However, these systems do not allow one to study the influence of non-integer dimensions on the electronic properties. Geometric electronic fractals, in which electrons are confined to a self-similar fractal geometry with a dimension between one and two, have been studied only from a theoretical perspective. For these fractals, a recurrent pattern in the density of states as well as extended and localized electronic states were predicted[19–22]. Recently, simulations of quantum transport in fractals revealed that the conductance fluctuations are related to the fractal dimension[23], and that the conductance in a Sierpiński fractal shows scale-invariant properties[24–26].

Here, we report how to construct and characterize, in a controlled fashion, a fractal lattice with electrons: the electrons that reside on a Cu(111) surface are confined to a self-similar Sierpiński geometry through atomic manipulation of CO molecules on the Cu(111) surface. The manipulation of surface-state electrons by adsorbates has been pioneered by Crommie et al.[27] and has been used to create electronic lattices 'on demand', such as a molecular graphene[2], an electronic Lieb lattice[3,28], a checkerboard and stripe-shaped lattice[29], and a quasiperiodic Penrose tiling[4]. We characterized the first three generations of an electronic Sierpiński triangle by scanning tunnelling microscopy and spectroscopy, acquiring the spatially and energy-resolved electronic local density of states (LDOS). These results were corroborated by muffin-tin calculations as well as tight-binding simulations based on artificial atomic *s*-orbitals coupled in the Sierpiński geometry.

The Sierpiński triangle with Hausdorff dimension $\log(3)/\log(2) = 1.58$ is presented in Fig. 1a. We define atomic sites at the corners and in the centre of the light blue triangles, as shown in Fig. 1b for the first generation $G(1)$[10,30]. $G(1)$ has three inequivalent atomic sites, indicated in red, green and blue, which differ by their connectivity. A triangle of generation $G(N)$ consists of three triangles $G(N-1)$, sharing the red corner sites. The surface-state electrons of Cu(111) are confined to the atomic sites by adsorbed CO molecules, acting as repulsive scatterers. Figure 1c shows the experimental realization of the first three generations of the Sierpiński triangle and Fig. 1d shows the relation with the artificial atomic sites. The distance between neighbouring sites is 1.1 nm, such that the electronic structure of the fractal will emerge in an experimentally suitable energy range[2].

Figure 1e presents the experimental LDOS at the red, blue and green atomic sites in the $G(3)$ Sierpiński triangle (indicated by the open circles in Fig. 1c). The differential conductance ($\mathrm{d}I/\mathrm{d}V$) spectra were normalized by the average spectrum taken on the bare Cu(111) surface, similar to ref. [2]. The onset of the surface-state band is located at $V = -0.45$ V. We focus on the bias window between -0.4 V and 0.3 V. Around $V = -0.3$ V the LDOS on the red, green and blue sites is nearly equal, whereas slightly above $V = -0.2$ V, the red sites exhibit a distinct minimum, while the green and blue sites show a considerably higher LDOS. At $V = -0.1$ V, the blue sites show a minimum, whereas the red and green sites exhibit a pronounced maximum in the LDOS. At $V = +0.1$ V, the blue sites show a larger peak in the differential conductance, whereas the green and red sites exhibit a smaller peak. The experimental LDOS is in good agreement with both the tight-binding (see Fig. 1f) and muffin-tin simulations (see Supplementary Information). This finding corroborates that our design leads to the desired confinement of the two-dimensional electron gas to the atomic sites of the Sierpiński geometry. In addition, it allows us to characterize the wavefunctions of the chosen Sierpiński geometry in detail.

[1]Institute for Theoretical Physics, Utrecht University, Utrecht, the Netherlands. [2]Debye Institute for Nanomaterials Science, Utrecht University, Utrecht, the Netherlands. [3]These authors contributed equally to this work: S. N. Kempkes, M. R. Slot. *e-mail: i.swart@uu.nl; c.demoraisSmith@uu.nl

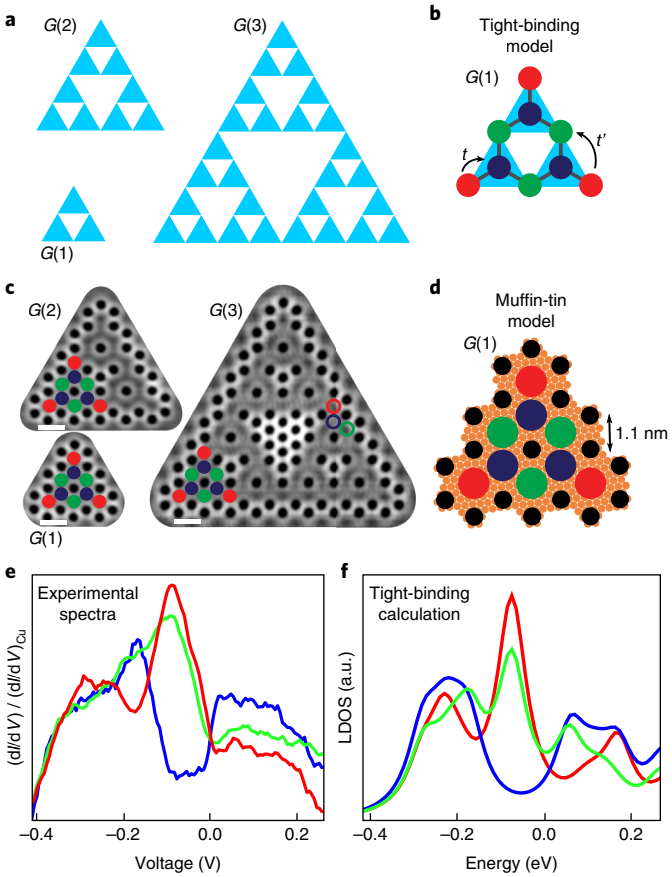

Fig. 1 | Geometry of the Sierpiński triangle fractal. a, Schematic of Sierpiński triangles of the first three generations *G*(1)–*G*(3). *G*(1) is an equilateral triangle subdivided into four identical triangles, from which the centre triangle is removed. Three *G*(1) (*G*(2)) triangles are combined to form a *G*(2) (*G*(3)) triangle. **b**, Geometry of a *G*(1) Sierpiński triangle with red, green and blue atomic sites. *t* and *t*′ indicate nearest-neighbour and next-nearest-neighbour hopping between the sites in the tight-binding model. **c**, Constant-current STM images of the realized *G*(1)–*G*(3) Sierpiński triangles. The atomic sites of one *G*(1) building block are indicated as a guide to the eye. Imaging parameters: $I = 1$ nA, $V = 1$ V for *G*(1) and *G*(2) and 0.30 V for *G*(3). Scale bar, 2 nm. **d**, The configuration of CO molecules (black) on Cu(111) to confine the surface-state electrons to the atomic sites of the Sierpiński triangle. **e**, Normalized differential conductance spectra acquired above the positions of red, blue and green open circles in **c** (and equivalent positions). **f**, LDOS at the same positions, simulated using a tight-binding model with $t = 0.12$ eV, $t' = 0.01$ eV and an overlap $s = 0.2$. a.u., arbitrary units.

Figure 2 shows experimental wavefunction maps obtained at different bias voltages and a comparison with simulations using a tight-binding and muffin-tin model. In a thought experiment, we will discuss how electrons can be transported across the set-up between a source and a drain at arbitrary positions. At a bias voltage of −0.325 V, the red (R), green (G) and blue (B) sites all have a high LDOS, and this also holds between the sites. Hence, from a chemical perspective, this wavefunction has strong bonding character, yielding an excellent conductivity from source to drain along (R–B–G–B–R)-pathways. At $V = -0.2$ V, the red sites that connect the *G*(1) triangles have a low amplitude: the wavefunction of the *G*(3) triangle partitions into nine parts, each corresponding to a *G*(1) triangle. The self-similar Sierpiński geometry thus leads to a subdivision of a fully bonding wavefunction delocalized over the *G*(3) Sierpiński triangle at −0.325 V in self-similar *G*(1) parts at −0.2 V, demonstrating self-similar properties of the LDOS itself. At the latter bias voltage, the conductivity along (R–B–G–B–R)-pathways suffers from the lower amplitude on the red sites (except the red corner sites). At $V = -0.1$ V, the LDOS shows a marked minimum on the blue sites and a peak at the green and red sites. From the tight-binding calculation, we find that the wavefunction has nodes on the blue sites, corresponding to a non-bonding molecular orbital from a chemical perspective. It is clear that the conductivity along the (R–B–G–B–R)-pathway mediated by nearest-neighbour hopping has vanished, and that electrons have to perform next-nearest-neighbour hopping between the red and green sites to propagate. These results connect with the theoretically calculated transmission of a Sierpiński carpet on a hexagonal lattice, which exhibits a gap in the conductivity although there is a high DOS in the system[23]. Finally, at $V = +0.1$ V, all blue sites in the *G*(3) Sierpiński structure have a high amplitude, whereas the red and green sites exhibit a low amplitude. Again, the conductivity between source and drain is suppressed. We note that the LDOS maps of the three generations *G*(1)–*G*(3) show the same features (see Supplementary Information), which is a consequence of the self-similarity of the geometry. We study this scale-invariance of the wavefunction in more detail with the box-counting method.

To determine whether the electronic wavefunctions inside the Sierpiński structure inherit the scaling properties of the Sierpiński geometry, we determine the fractal dimension of the wavefunction maps at different energies following the procedure in ref. [31]. We calculate the box-counting dimension (also called the Minkowski–Bouligand dimension) for both the experimental and simulated muffin-tin LDOS maps using $D = \lim_{r \to 0} \frac{\log N(r)}{\log(1/r)}$, with N the number of squares on a square grid required to cover the contributing LDOS and r the side length of these squares. In this procedure the wavefunction maps are positioned on a 360 × 360 pixel square grid. The parts of the wavefunction maps that are in the regions containing an agglomeration of CO molecules are excluded by applying a mask. Further, we choose a threshold (55%, 65% and 75% of the maximum LDOS) above which the LDOS contributes to define a binary image. Finally, the box-counting dimension of this image is calculated. The number of boxes N is counted for 21 box sizes ranging from 1 to 90 pixels. Subsequently, the fractal dimension is given by the slope of the log–log plot for $N(r)$. Details can be found in the Supplementary Information. A typical log–log plot is presented in Fig. 3a, where the inset shows the binarized experimental LDOS map at $V = -0.325$ V. The red slope is calculated for the largest 11 boxes and the blue slope for the smallest 10 boxes. Figure 3b shows the box-counting dimension obtained from these red slopes for the experimental (dark red) and theoretical (light red) wavefunction maps acquired at various energies. For comparison, we also show the dimension obtained for the wavefunction maps of a square lattice (dark and light green, for the experiment and theory, respectively), realized in the same way and measured in the same energy window[3]. The difference between the experimental and simulated maps is ascribed to a more gradual contrast in the simulation, where also contributions of the tip density of states do not play a role. It can be clearly seen that the box-counting dimension of the Sierpiński triangle is close to the theoretical Hausdorff dimension 1.58 (red solid line), whereas the square lattice has a dimension close to 2 (green solid line). When calculating the box-counting dimension for the blue slopes for the Sierpiński triangle, we find the results shown in Fig. 3c. When using the 10 smallest boxes, the analysis yields higher values of the dimensions for the fractal, but they are still well below 2 and well below the values obtained for the square lattice. This behaviour is well understood (see Supplementary Information). From these results and an additional scaling analysis shown in the Supplementary Information, we conclude that the wavefunctions inherit the fractal dimension and therefore the scaling properties of

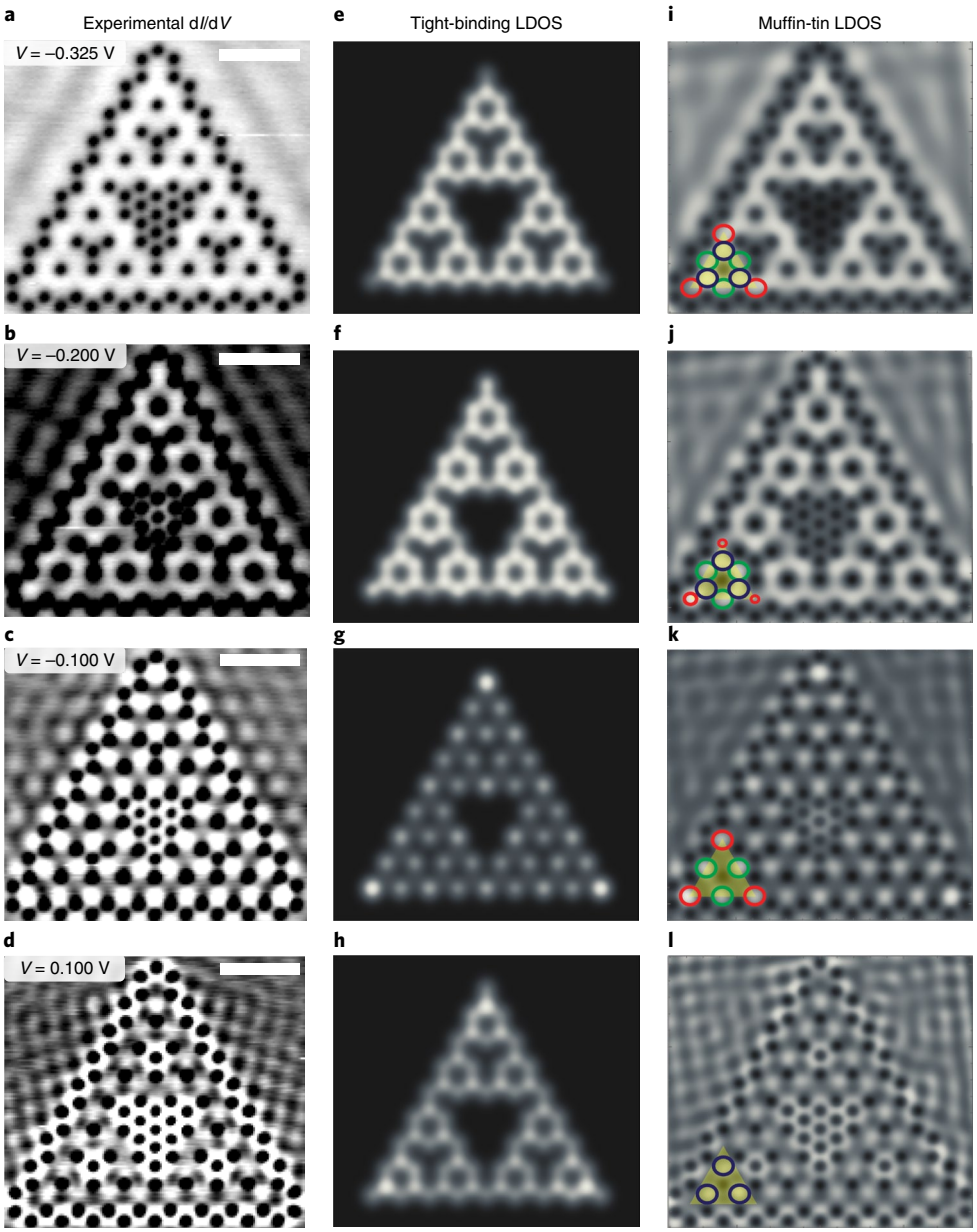

Fig. 2 | Wavefunction mapping. a–d, Differential conductance maps acquired above a $G(3)$ Sierpiński triangle at bias voltages −0.325 V, −0.200 V, −0.100 V and +0.100 V. Scale bar: 5 nm. **e–h**, LDOS maps at these energies calculated using the tight-binding model. **i–l**, LDOS maps simulated using the muffin-tin approximation. As a guide to the eye, a $G(1)$ building block is indicated, in which a larger radius of the circles corresponds to a larger LDOS at an atomic site, whereas no circle indicates a node in the LDOS.

the geometry to which they are confined, and that this dimension can be non-integer.

Finally, we show how the self-similarity of the wavefunction maps is reflected in momentum space. The Fourier-transformed wavefunction map at $V = -325$ mV (Fig. 4a) exhibits distinct maxima at $k = 1.9\,\mathrm{nm}^{-1}$ (turquoise), $k = 1.0\,\mathrm{nm}^{-1}$ (red) and $k = 0.5\,\mathrm{nm}^{-1}$ (yellow). These maxima correspond to the next-nearest-neighbour distances between the artificial atomic sites (see Fig. 1), the side of a $G(1)$ triangle, and the side of a $G(2)$ triangle in real space, respectively. We then transform parts of the Fourier map back into real space (Fig. 4b–d). The data inside the turquoise circle recover the full $G(3)$ Sierpiński triangle, as shown in Fig. 4b. Transforming the values inside the red circle, however, results in a Sierpiński triangle of generation 2, while the size is retained (see Fig. 4c). Analogously, transforming the data inside the yellow circle yield a first-generation Sierpiński triangle (Fig. 4d). This shows that the $G(3)$ wavefunction contains Fourier terms of the previous generations. The self-similar features of the Sierpiński triangle are thus inherently encoded in momentum space.

We have demonstrated a rational concept of building electronic wavefunctions with a fractional dimension from artificial atomic sites that couple in a controlled way. We discussed the wavefunctions that form by coupling the s-orbitals of artificial atoms in the single-electron regime. Although this study represents the simplest case, it already exhibits several aspects of fractal confinement. The emergent fractionalization of the wavefunction at the single-particle level has profound implications and opens a series of interesting questions for future investigation: Do electrons in $D = 1.58$ behave like Luttinger liquids? Do they exhibit the fractional quantum Hall effect in the presence of a strong perpendicular

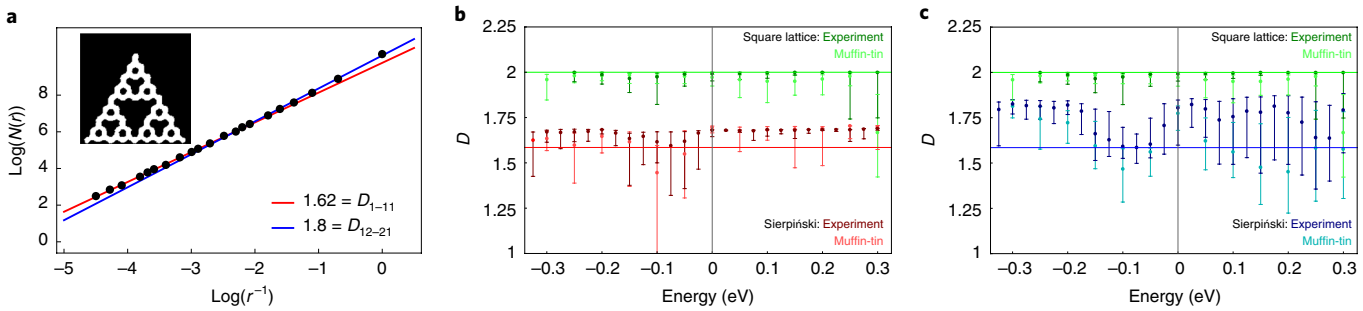

Fig. 3 | Fractal dimension of the Sierpiński wavefunction maps. a, The box-counting dimension of the experimental wavefunction map acquired at $V = -0.325$ V is obtained from the slope of log(N) versus log(r^{-1}), where either the first 11 datapoints starting from the left (largest boxes, red slope) or the last 10 datapoints (smallest boxes, blue slope) are taken into account. Inset: binarized and masked map of the experimental LDOS obtained with a binarization threshold of 65%. **b**, Determination of the fractal dimensions of the LDOS of the $G(3)$ Sierpiński triangle (red) using the 11 largest boxes (red slopes) and comparison with the 2D square lattice from ref. [3] (green) for the experimental (dark) and muffin-tin (light) wavefunction maps with a threshold of 65%. The error bars display the error due to the choice of the binarization threshold, indicating the fractal dimension at LDOS thresholds of 55% (top) and 75% (bottom). The solid lines show the geometric Sierpiński Hausdorff dimension ($D = 1.58$) and that of the square lattice ($D = 2$). **c**, The box-counting dimension of the wavefunction maps when the last 10 datapoints are taken into account for the Sierpiński triangle (blue).

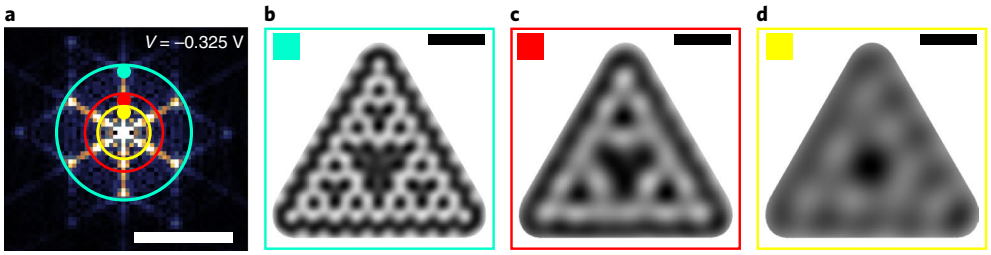

Fig. 4 | Fourier analysis of wavefunction maps. a, Fourier transform of the experimental differential conductance map at −0.325 V. The k-values outside the circles are excluded from the Fourier-filtered images in **b**–**d**. Scale bar: $k = 3$ nm^{-1}. **b**–**d**, Wavefunction map at −0.325 V after Fourier filtering, including merely the k-values within the turquoise (**b**), red (**c**) and yellow (**d**) circles indicated in **a**. Scale bar: 5 nm.

magnetic field, or is the behaviour hybrid between 1D and 2D? How does charge fractionalization manifest when the wavefunction is itself already fractional? Recent theoretical work already addresses parts of these questions and corroborates the potential of electrons in fractal lattices, showing that the Sierpiński carpet and gasket host topologically protected states in the presence of a perpendicular magnetic field[32]. Furthermore, the design of artificial-atom quantum dots coupled in a fractal geometry can also be implemented in semiconductor technology, thus making it possible to perform spectroscopy and transport experiments under controlled electron density. This would form a versatile platform to explore fractal electronics with several internal degrees of freedom, such as orbital type, Coulomb and spin–orbit interactions, as well as external electric and magnetic fields.

Online content

Any methods, additional references, Nature Research reporting summaries, source data, statements of data availability and associated accession codes are available at https://doi.org/10.1038/s41567-018-0328-0

Received: 17 July 2018; Accepted: 19 September 2018;
Published online: 12 November 2018

References

1. Mandelbrot, B. B. *The Fractal Geometry of Nature* (W. H. Freeman, San Francisco, 1982).
2. Gomes, K. K., Mar, W., Ko, W., Guinea, F. & Manoharan, H. C. Designer Dirac fermions and topological phases in molecular graphene. *Nature* **483**, 306–310 (2012).
3. Slot, M. R. et al. Experimental realization and characterization of an electronic Lieb lattice. *Nat. Phys.* **13**, 672–676 (2017).
4. Collins, L. C., Witte, T. G., Silverman, R., Green, D. B. & Gomes, K. K. Imaging quasiperiodic electronic states in a synthetic Penrose tiling. *Nat. Commun.* **8**, 15961 (2017).
5. Newkome, G. R. et al. Nanoassembly of a fractal polymer: A molecular 'Sierpinski hexagonal gasket'. *Science* **312**, 1782–1785 (2006).
6. Yu, B. Analysis of flow in fractal porous media. *Appl. Mech. Rev.* **61**, 050801 (2008).
7. Dubal, D. P., Ayyad, O., Ruiz, V. & Gomez-Romero, P. Hybrid energy storage: the merging of battery and supercapacitor chemistries. *Chem. Soc. Rev.* **44**, 1777–1790 (2015).
8. Fan, J. A. et al. Fractal design concepts for stretchable electronics. *Nat. Commun.* **5**, 3266 (2014).
9. Rothemund, P. W., Papadakis, N. & Winfree, E. Algorithmic self-assembly of DNA Sierpinski triangles. *PLoS Biol.* **2**, e424 (2004).
10. Shang, J. et al. Assembling molecular Sierpiński triangle fractals. *Nat. Chem.* **7**, 389–393 (2015).
11. Li, C. et al. Construction of Sierpiński triangles up to the fifth order. *J. Amer. Chem. Soc.* **139**, 13749–13753 (2017).
12. De Nicola, F. et al. Multiband plasmonic Sierpinski carpet fractal antennas. *ACS Photon.* **5**, 2418–2425 (2018).
13. Hofstadter, D. R. Energy levels and wave functions of Bloch electrons in rational and irrational magnetic fields. *Phys. Rev. B* **14**, 2239–2249 (1976).
14. Pan, W. et al. Fractional quantum Hall effect of composite fermions. *Phys. Rev. Lett.* **90**, 016801 (2003).
15. Goerbig, M. O., Lederer, P. & Smith, C. M. On the self-similarity in quantum Hall systems. *Europhys. Lett.* **68**, 72–78 (2004).
16. Morgenstern, M., Klijn, J., Meyer, C. & Wiesendanger, R. Real-space observation of drift states in a two-dimensional electron system at high magnetic fields. *Phys. Rev. Lett.* **90**, 056804 (2003).
17. Richardella, A. et al. Visualizing critical correlations near the metal–insulator transition in $Ga_{1-x}Mn_xAs$. *Science* **327**, 665–669 (2010).
18. Evers, F. & Mirlin, A. D. Anderson transitions. *Rev. Mod. Phys.* **80**, 1355–1417 (2008).

19. Domany, E., Alexander, S., Bensimon, D. & Kadanoff, L. P. Solutions to the Schrödinger equation on some fractal lattices. *Phys. Rev. B* **28**, 3110–3123 (1983).
20. Ghez, J., Wang, Y. Y., Rammal, R., Pannetier, B. & Bellissard, J. Band spectrum for an electron on a Sierpinski gasket in a magnetic field. *Solid State Commun.* **64**, 1291–1294 (1987).
21. Andrade, R. F. S. & Schellnhuber, H. J. Exact treatment of quantum states on a fractal. *Europhys. Lett.* **10**, 73–78 (1989).
22. Wang, X. R. Localization in fractal spaces: Exact results on the Sierpinski gasket. *Phys. Rev. B* **51**, 9310–9313 (1995).
23. van Veen, E., Yuan, S., Katsnelson, M. I., Polini, M. & Tomadin, A. Quantum transport in Sierpinski carpets. *Phys. Rev. B* **93**, 115428 (2016).
24. Chakrabarti, A. & Bhattacharyya, B. Sierpinski gasket in a magnetic field: electron states and transmission characteristics. *Phys. Rev. B* **56**, 13768–13773 (1997).
25. Liu, Y., Hou, Z., Hui, P. M. & Sritrakool, W. Electronic transport properties of Sierpinski lattices. *Phys. Rev. B* **60**, 13444–13452 (1999).
26. Lin, Z., Cao, Y., Liu, Y. & Hui, P. M. Electronic transport properties of Sierpinski lattices in a magnetic field. *Phys. Rev. B* **66**, 045311 (2002).
27. Crommie, M. F., Lutz, C. P. & Eigler, D. M. Confinement of electrons to quantum corrals on a metal. *Surf. Sci.* **262**, 218–220 (1993).
28. Drost, R., Ojanen, T., Harju, A. & Liljeroth, P. Topological states in engineered atomic lattices. *Nat. Phys.* **13**, 668–671 (2017).
29. Girovsky, J. et al. Emergence of quasiparticle Bloch states in artificial crystals crafted atom-by-atom. *SciPost Phys.* **2**, 020 (2017).
30. Oftadeh, R., Haghpanah, B., Vella, D., Boudaoud, A. & Vaziri, A. Optimal fractal-like hierarchical honeycombs. *Phys. Rev. Lett.* **113**, 104301 (2014).
31. Foroutan-pour, K., Dutilleul, P. & Smith, D. Advances in the implementation of the box-counting method of fractal dimension estimation. *Appl. Math. Comput.* **105**, 195–210 (1999).
32. Brzezińska, M., Cook, A. M. & Neupert, T. Topology in the Sierpiński–Hofstadter problem. Preprint at https://arXiv.org/abs/1807.00367 (2018).

Acknowledgements

We thank G.C.P. van Miert for the discussions. We acknowledge funding from NWO via grants 16PR3245 and DDC13, as well as an ERC Advanced Grant 'FIRSTSTEP' 692691.

Author contributions

S.N.K. did the calculations under the supervision of C.M.S. The experiments were performed by M.R.S. with contributions from S.E.F. and S.J.M.Z. under the supervision of I.S. and D.V. All authors contributed to the interpretation of the data and to the manuscript.

Additional information

Supplementary information is available for this paper at https://doi.org/10.1038/s41567-018-0328-0.

Reprints and permissions information is available at www.nature.com/reprints.

Correspondence and requests for materials should be addressed to I.S. or C.M.S.

Publisher's note: Springer Nature remains neutral with regard to jurisdictional claims in published maps and institutional affiliations.

Methods

Scanning tunnelling microscope experiments. The scanning tunnelling microscopy and spectroscopy experiments were performed in a Scienta Omicron LT-STM system at a temperature of 4.5 K and a base pressure around 10^{-10}–10^{-9} mbar. A clean Cu(111) crystal, prepared by multiple cycles of Ar^+ sputtering and annealing, was cooled down in the scanning tunnelling microscope head. Carbon monoxide was leaked into the chamber at $p \approx 3.10^{-8}$ mbar for 3 min and adsorbed at the cold Cu(111) surface. A Cu-coated tungsten tip was used for both the assembly and the characterization of the fractal. The CO manipulation was performed in feedback at $I = 60$ nA and $V = 50$ mV, comparable to previously reported values[33,34], and was partly automated using an in-house-developed program. Scanning tunnelling microscopy was performed in constant-current mode. A standard lock-in amplifier was used to acquire differential conductance spectra ($f = 973$ Hz, modulation amplitude 5 mV r.m.s.) and maps ($f = 273$ Hz, modulation amplitude 10 mV r.m.s.) in constant-height mode. The contrast of the experimental wavefunction maps as displayed in Fig. 2 was adjusted using the software Gwyddion. For the box-counting analysis of the experimental wavefunction maps (Fig. 3), Fourier-smoothed images were used with no further adjustments of the contrast. The Fourier analysis (Fig. 4) was performed using the same software.

Tight-binding calculations. The atomic sites in the first three generations of the Sierpiński triangle[35] are modelled as *s*-orbitals, for which electron hopping between nearest-neighbour and next-nearest-neighbour sites is defined. The parameters used are $e_s = -0.1$ eV for the on-site energy, $t = 0.12$ eV for the nearest-neighbour hopping and $t'/t = 0.08$ for the next-nearest-neighbour hopping, similar to previously reported values[2]. Furthermore, we included an overlap integral $s = 0.2$ between nearest-neighbours and solved the generalized eigenvalue equation $H|\psi\rangle = E\mathcal{S}|\psi\rangle$, where $\mathcal{S}$ is the overlap-integral matrix. The LDOS is calculated at each specific atomic site and a Lorentzian energy-level broadening of $\Gamma = 0.8$ eV is included to account for bulk scattering. For the simulation of the LDOS maps, the same energy-level broadening was used and the LDOS at each site was multiplied with a Gaussian wavefunction of width $\sigma = 0.65a$, where $a = 1.1$ nm is the distance between two neighbouring sites.

Muffin-tin calculations. The surface-state electrons of Cu(111) are considered to form a 2D electron gas confined between the CO molecules, which are modelled as filled circles with a repulsive potential of 0.9 eV and radius $R = 0.55a/2$. The Schrödinger equation is solved for this particular potential landscape, and a Lorentzian broadening of $\Gamma = 0.8$ eV is used to account for the bulk scattering.

Box-counting method. The Minkowski–Bouligand[36] or box-counting method is a useful tool to determine the fractal dimension of a certain image, but has to be handled and interpreted with care. In particular, as has been shown previously[31], the size of the boxes needs to be chosen within certain length scales. More specifically, the largest box should not be more than 25% of the entire image side and the smallest box is chosen to be the point at which the slope starts to deviate from the linear regime in the $\log(N)$ versus $\log(1/r)$ plot. Due to experimental limitations, it is not always possible to fully 'block' certain areas using the CO/Cu(111) platform. Redundant features that are not part of the fractal set, such as the Friedel oscillations surrounding the Sierpiński triangle and the LDOS between the closely packed CO molecules in the centres of the $G(2)$ and $G(3)$ Sierpiński triangles, were removed by applying a mask (see Supplementary Information). The masks serve as a proxy for the areas that should be excluded from future experiments using other platforms (for example, by etching or gating those areas). Furthermore, the wavefunction maps are not binary, and therefore it is necessary to specify the LDOS threshold value above which the pixels are part of the fractal set. This binarization threshold is a certain percentage of the maximum LDOS of the masked wavefunction map at a specific energy. The error introduced by the choice of the threshold is accounted for by performing the calculation procedure for the threshold percentages of 55%, 65% and 75% indicated by the top, centre and bottom of the error bar, respectively (see Supplementary Information). In addition to the box sizes chosen in the main text, the results for other box sizes are presented in the Supplementary Information.

Data availability

The experimental and simulated images used in the box-counting analysis, as well as the code, have been published (https://doi.org/10.24416/UU01-N90LX5). The data can be accessed using open-source tools.

References

33. Meyer, G. et al. Controlled manipulation of atoms and small molecules with a low temperature scanning tunneling microscope. *Single Mol.* **1**, 79–86 (2000).
34. Celotta, R. J. et al. Invited Article: Autonomous assembly of atomically perfect nanostructures using a scanning tunneling microscope. *Rev. Sci. Instrum.* **85**, 121301 (2014).
35. Sierpiński, W. Sur une courbe dont tout point est un point de ramification. *Comptes Rendus Acad. Sci.* **160**, 302–315 (1915).
36. Bouligand, G. Sur la notion d'ordre de mesure d'un ensemble plan. *Bull. Sci. Math* **2**, 185–192 (1929).